Interaction of torsion and lateral bending in aircraft nose landing gear shimmy

Thota, P.; Krauskopf, B.; Lowenberg, M.

published in
Nonlinear Dynamics
2009

DOI (link to publisher)
10.1007/s11071-008-9455-y

document version
Publisher's PDF, also known as Version of record

Nonlinear Dyn (2009) 57: 455–467
DOI 10.1007/s11071-008-9455-y

ORIGINAL PAPER

Interaction of torsion and lateral bending in aircraft nose landing gear shimmy

Phanikrishna Thota · Bernd Krauskopf · Mark Lowenberg

Received: 1 May 2008 / Accepted: 17 November 2008 / Published online: 9 December 2008

Abstract In this paper we consider the onset of shimmy oscillations of an aircraft nose landing gear. To this end we develop and study a mathematical model with torsional and lateral bending modes that are coupled through a wheel-mounted elastic tyre. The geometric effects of a positive rake angle are fully incorporated into the resulting five-dimensional ordinary differential equation model. A bifurcation analysis in terms of the forward velocity and the vertical force on the gear reveals routes to different types of shimmy oscillations. In particular, we find regions of stable torsional and stable lateral shimmy oscillations, as well as transient quasiperiodic shimmy where both modes are excited.

Keywords Aircraft dynamics · Shimmy oscillations · Mode interaction · Quasiperiodic motion

P. Thota (✉) · B. Krauskopf
Department of Engineering Mathematics, University of Bristol, Queen's Building, University Walk, Bristol BS8 1TR, UK
e-mail: phani.thota@bris.ac.uk

M. Lowenberg
Department of Aerospace Engineering, University of Bristol, Queen's Building, University Walk, Bristol BS8 1TR, UK

1 Introduction

Lateral, unwanted oscillations during the motion of wheeled vehicles, such as aircraft, motorcycles, cars and trailers, are undesirable due to their detrimental effects on the safety as well as on the costs involved in the maintenance of the vehicle. Such oscillations are generally referred to as *shimmy oscillations*. One of the earliest documented evidence of shimmy was reported by Broulhiet [3], who investigated the dynamics of cars. The concept of side slip that he introduced still forms the basis for the understanding of shimmy oscillations in a wide range of wheeled vehicles. Another milestone for shimmy research was the seminal work of von Schlippe and Dietrich [17] on tyre mechanics and its influence on shimmy. Shimmy has been studied in general wheeled vehicles, including cars, pulled trailers, motorcycles and aircraft; see, for example, the overview papers by Dengler et al. [4], Smiley [13] and Pritchard [12] as an entry point to the literature.

Of particular interest for our study is the work by Pacejka [10, 11] and by Stépán [15, 16], who consider a pulled trailer—a system that is characterized by a large caster length (mechanical trail) with zero rake angle and weak damping, and possible freeplay at the kingpin. Pacejka [10, 11] found experimentally and in a 13th-order model that shimmy may occur for a wide range of velocities and may be associated with sudden jumps into and out of shimmy when the velocity

is changed. Furthermore, he found the first example of quasiperiodic shimmy in the form of beating oscillations where also the translational mode at the kingpin is excited. Sudden jumps from straight-line motion (no shimmy) of the tyre to large amplitude shimmy with only a very small variation in a system parameter were also found by Stépán [16]. Furthermore, in [15] he systematically investigates quasiperiodic shimmy oscillations and shows that in his pulled trailer setup the second frequency is due to a memory effect associated with the rolling tyre. This type of tyre dynamics must be modeled mathematically by a set of time-delayed differential equations. In separate work, Takács and Stépán [18] found quasiperiodic shimmy in an experimental setup resembling a pulled trailer; the experimental observations are also verified by comparison with a time-delayed mathematical model.

In this paper we consider the onset of shimmy oscillations for the case of an aircraft nose landing gear—an issue that is essentially as old as aircraft themselves. While there are certain commonalities, there are important differences between different types of vehicles, which are crucial for the dynamics and the onset of shimmy oscillations. The nose landing gear of a typical midsize commercial passenger aircraft has three main vibrational modes: a torsional mode corresponding to the rotation about the strut axis, a lateral mode that is representative of vibrations of the gear about an axis passing through the fuselage centerline, and a vertical mode associated with the shock dampers of the gear (which are generally called oleos in the context of aircraft landing gears). These three modes of vibration are coupled via the tyre-ground interaction and play an important role in the occurrence of shimmy in aircraft. In contrast to pulled trailers, an aircraft nose landing gear generally features a nonzero rake angle and its torsional mode is very strongly damped.

Initial work in the early 1930s on the dynamic stability of aircraft on the ground concentrated on the excitation of the vertical mode via roughness of the ground. See the overview paper by Dengler et al. [4] for a discussion of the early literature on how the vertical mode may interact either with the torsional or with the lateral mode. By contrast, the vertical mode of a commercial aircraft is generally sufficiently damped so that it does not get excited on today's smooth runways or taxiways. Nevertheless, shimmy oscillations may still occur in aircraft landing gears, and this has been studied experimentally, by means of linear stability analysis and by numerical simulation; see the reviews [1, 2, 6, 8]. Smiley [13] studied shimmy for three different landing gear structures. While one of the cases had a nonzero rake angle, its nonlinear geometric effects were not included in the model. The paper [13] contains linear stability analysis of a landing gear model and discusses a systematic way of modeling the geometrical aspects of the strut. More recently, Somieski [14] studied shimmy as a nonlinear phenomenon of a nonlinear set of ODEs describing a nose landing gear with zero rake angle. Here, time domain analysis showed a case of supercritical Hopf bifurcation leading to a set of stable limit cycles past the bifurcation point. Woerner and Noel [20] describe the main cause of shimmy as the energy transfer from the contact force between the tyres and the ground to the vibrational modes of the landing gear system whose stability depends on the damping and stiffness characteristics of tyres and the supporting structure. They also studied the change in the frequency of different vibrational modes of a typical nose landing gear as a function of swivel friction and forward velocity. This suggests that coupled motion can occur due to resonance phenomena under variations in the forward velocity, leading to high-amplitude shimmy oscillations.

The focus of this work is the interaction between the torsional mode and the lateral mode, which are strongly coupled via the nonlinear restoring force of the elastic tyre. Specifically, we develop a mathematical model in the form of a five-dimensional system of ordinary differential equations for the two modes and the kinematic equation of the nonlinear tyre. Here we use a variant of the widely accepted *stretched string* model developed by von Schlippe [17], where we include the effect of lateral bending on the lateral deformation of the tyre. Importantly, we include in the model the geometric effects of a nonzero rake angle of the gear.

A bifurcation analysis of our mathematical model with the software package AUTO [5] reveals a two-parameter bifurcation diagram in the plane of forward velocity and vertical force on the gear. The main features of the bifurcation diagram are two curves of Hopf bifurcations, of the torsional mode and the lateral mode, respectively, which intersect at two double-Hopf points. These codimension-two points give rise to curves of torus bifurcations (or Neimark–Sacker bifurcations [7, 9]) that are associated with the emergence of quasiperiodic shimmy oscillations. Overall, we find a comprehensive picture of parameter re-

gions corresponding to stable straight-line motion, torsional, lateral and transient quasiperiodic shimmy oscillations.

The paper is organized as follows. In Sect. 2 we develop the mathematical model, which involves deriving the relevant coupling terms between the torsional and lateral modes via nonlinear tyre forces. Section 3 is devoted to the bifurcation analysis of the model. We first show selected one-parameter continuations in the forward velocity and then present the bifurcation diagram in the plane of forward velocity and vertical force on the gear; representative time series of different types of shimmy oscillations are also presented. Section 4 summarizes and discusses directions of future research.

2 Model of a nose landing gear with torsional and lateral dynamics

The nose landing gear of an aircraft consists of a strut that is attached to the aircraft fuselage and coupled to the ground via one or more wheels with flexible tyres. We consider here a nose landing gear as sketched in Fig. 1. Throughout this work we use one of the conventionally accepted coordinate systems for aircraft analysis. Specifically, the positive X-axis points towards the backward direction of the aircraft, the Z-axis is the upward normal to the (flat) ground, and the Y-axis completes the right-handed coordinate system.

The strut is able to rotate about its axis S, which gives rise to a steering angle ψ. The wheel axle, offset from the strut axis by a mechanical trail (caster) of length e, supports a wheel with tyre of radius R. Importantly, the strut axis is inclined to the vertical at a rake angle ϕ. The aircraft body is modeled as a block of mass exerting a vertical force F_z on the gear, which is moving at a fixed horizontal velocity V. Apart from torsional motion as described by the steering angle ψ, we also consider lateral bending motion of the gear assembly about the X-axis. The lateral motion is modeled (in first-order approximation) by an angle δ that the strut makes with the zero position. These two geometric degrees of freedom are coupled via the lateral deformation λ of the tyre. The wheel–ground interaction is modeled by the well-established stretched string model from [17] of an elastic tyre, which we modified to incorporate the deformation due to the lateral bending mode.

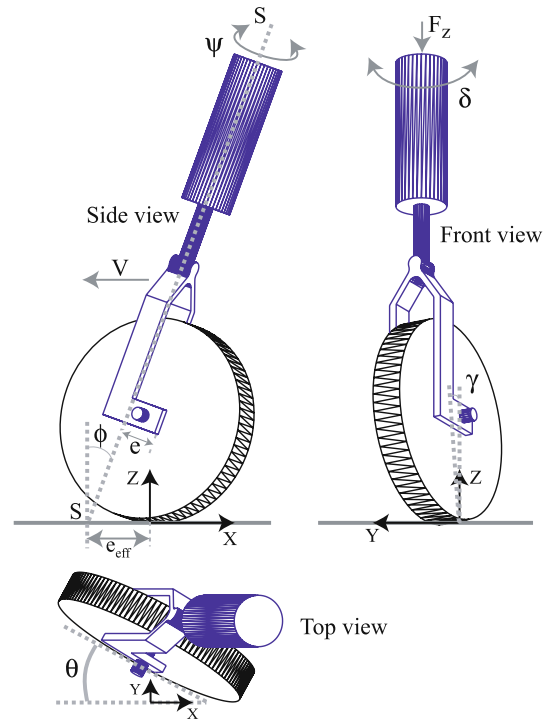

Fig. 1 Schematic side, front and top views of an aircraft nose landing gear

The structure shown in Fig. 1 closely resembles the nose landing gear of an aircraft, which is characterized by a moderate rake angle (about 10 degrees), a small caster length e (about 0.1 m for a midsize passenger aircraft), and large stiffness and damping of the torsional mode ψ and the lateral mode δ due to the steering mechanism. Specifically, we use throughout realistic parameters for geometry and tyre taken from [14] and summarized in Table 1. For comparison, motorcycles generally have large rake angles (possibly even larger than 30 degrees) and a small caster length, while trailers have zero rake angle and a long caster length (up to several metres). Importantly, in both motorcycles and trailers the torsional mode ψ (corresponding here to rotation around the steering axis or kingpin, respectively) is only weakly damped, which makes them quite prone to shimmy oscillations.

The presence of a nonzero rake angle ϕ is incorporated into our model because it has several important geometrical effects in an aircraft nose landing gear. First, it induces an effective caster length e_{eff} [19], which is given by

$$e_{\mathrm{eff}} = e\cos\phi + (R + e\sin\phi)\tan\phi. \tag{1}$$

Table 1 System parameters and their values as used in the modeling

Symbol	Parameter	Value	
	Structure parameters		
e	caster length	0.12	m
l_g	gear height	2.5	m
k_ψ	torsional stiffness of strut	3.8×10^5	N m rad^{-1}
c_ψ	torsional damping of strut	300.0	N m s rad^{-1}
I_z	moment of inertia of strut w.r.t. Z-axis	100.0	kg m^2
k_δ	lateral bending stiffness of strut	6.1×10^6	N m rad^{-1}
c_δ	lateral bending damping of strut	300.0	N m s rad^{-1}
I_x	moment of inertia of strut w.r.t. X-axis	600.0	kg m^2
ϕ	rake angle	0.1571	rad (9°)
	Tyre parameters		
R	radius of nose wheel	0.362	m
h	contact patch length	0.1	m
c_λ	damping coefficient of elastic tyre	570.0	N m^{2}rad^{-1}
k_α	self-aligning coefficient of elastic tyre	1.0	m rad^{-1}
k_λ	restoring coefficient of elastic tyre	0.002	rad^{-1}
L	relaxation length	0.3	m
α_m	self-aligning moment limit	0.1745	rad (10°)
	Continuation parameters		
F_z	vertical force on the gear	30.0–700.0	kN
V	forward velocity	10.0–180	m s^{-1}

Secondly, for a nonzero rake angle the swivel angle θ of the wheel with the ground is different from the steering angle ψ; namely, it is given by $\theta = \psi \cos\phi$. Thirdly, there is a tilt $\gamma = \psi \sin\phi$ of the wheel when the steering angle ψ is nonzero. The tilt γ contributes to the overall tilt of the wheel due to lateral bending motion as expressed by δ and both result in a lateral restoring force on the tyre. The point of application of this restoring force is ahead of the center of the contact patch. Depending on the tilt direction, this lateral tilt force may act in the same or in the opposite direction to the lateral restoring force created due to pure lateral distortion or torsional motion of the tyre. This can lead to an increase or decrease of the effective self-aligning moment responsible for stabilizing the shimmy oscillations. Since it is known to affect dynamics of motorcycles and cars more than aircraft tyres, we do not consider this force in the analysis.

Another effect of a nonzero rake angle is the increase in the moment that destabilizes the orientation of the gear. The vertical force F_z is offset from the $(X–Z)$ plane due to the effective caster length e_{eff}. This offset vertical force generates a moment, increased by the effect of the caster length, that acts to turn the gear about its strut axis. In the case of aircraft landing gears, the high torsional stiffness and damping about the strut axis resist this destabilizing moment. However, in the case of bicycles and motorcycles torsional stiffness and damping are negligibly small, so that this moment makes it very difficult to ride a bike when the handle bar is rotated by 180 degrees.

Taking into account torsional and lateral motion and their coupling through the elastic tyre, the equations for the landing gear model can be written in the form

$$I_z\ddot{\psi} + M_{K_\psi} + M_{D_\psi} + M_{F_1} + M_{D_\lambda} - F_z \sin(\phi) e_{\text{eff}} \sin(\theta) = 0, \tag{2}$$

$$I_x\ddot{\delta} + M_{K_\delta} + M_{D_\delta} + M_{\lambda_\delta} - F_z e_{\text{eff}} \sin(\theta) = 0, \tag{3}$$

$$\dot{\lambda} + \frac{V}{L}\lambda - V\sin(\theta) - l_g\dot{\delta}\cos(\delta) - (e_{\text{eff}} - h)\cos(\theta)\dot{\psi}\cos(\phi) = 0. \tag{4}$$

Equation (2) governs the torsional dynamics and (3) the lateral dynamics. Equation (4) comes from von

Schlippe's stretched string model [17]; it describes the nonlinear kinematic relationship between the steering angle ψ, lateral bending angle δ and the lateral deformation λ of the leading edge of the contact patch of the tyre. We now present a detailed description of the individual terms in (2)–(4) in the next sections.

2.1 Torsional mode of the landing gear

Equation (2) describes the torsional aspect of the landing gear dynamics. The moment M_{K_ψ} due to the torsional stiffness of the strut is a function of the steering angle ψ and is given by

$$M_{K_\psi} = k_\psi \psi, \tag{5}$$

and the moment M_{D_ψ} due to the torsional damping of the strut is a function of the angular velocity of the steering $\dot{\psi}$ and is given by

$$M_{D_\psi} = c_\psi \dot{\psi}, \tag{6}$$

where k_ψ and c_ψ are the torsional stiffness and damping coefficients of the strut, respectively. The last three terms in (2) model the tyre interaction with the ground. Specifically, the combined moment M_{F_1} due to the tyre's restoring force F_{K_λ} and self-aligning moment M_{K_α}, which are functions of the tyre's lateral deformation λ, is given by

$$M_{F_1} = M_{K_\alpha} + e_{\text{eff}} F_{K_\lambda}. \tag{7}$$

The self-aligning moment M_{K_α} is given by the piecewise continuous function [14]

$$M_{K_\alpha} = \begin{cases} k_\alpha \frac{\alpha_m}{\pi} \sin(\alpha \frac{\pi}{\alpha_m}) F_z & \text{if } |\alpha| \le \alpha_m, \\ 0 & \text{if } |\alpha| > \alpha_m, \end{cases} \tag{8}$$

and the lateral restoring force F_{K_λ} due to tyre deformation is given by

$$F_{K_\lambda} = k_\lambda \tan^{-1}\big(7.0\tan(\alpha)\big) \times \cos\big(0.95\tan^{-1}\big(7.0\tan(\alpha)\big)\big) F_z. \tag{9}$$

Here, k_α and k_λ are the torsional and lateral stiffnesses of the tyre. The slip angle α is related to the lateral deformation λ by $\alpha = \tan^{-1}(\lambda/L)$, where L is the *relaxation length* of the tyre. The rake angle ϕ enters into the model via the effective caster length as given in (1); note that $e_{\text{eff}} = e$ for $\phi = 0$. The constant α_m is the limit on the slip angle α beyond which the self-aligning moment is taken to be zero.

Finally, in (2), the moment M_{D_λ} due to the tyre's tread damping is given by

$$M_{D_\lambda} = \frac{c_\lambda \dot{\psi} \cos(\phi)}{V}, \tag{10}$$

where c_λ is the lateral damping coefficient of the tyre.

2.2 Lateral bending mode of the landing gear

Equation (3) describes the lateral bending motion of the landing gear assembly about the X-axis. The moment M_{K_δ} due to the stiffness of the strut acting against the lateral bending motion is a function of δ and is given as

$$M_{K_\delta} = k_\delta \delta, \tag{11}$$

where k_δ is the bending stiffness of the strut w.r.t. the rotation about the X-axis.

The moment M_{D_δ} due to the damping characteristics of the strut against the lateral motion is a function of $\dot{\delta}$ and is given as

$$M_{D_\delta} = c_\delta \dot{\delta}, \tag{12}$$

where c_δ is the damping coefficient of the lateral bending of the strut. The last two terms in (3) are contributions of the tyre forces to the lateral bending motion δ. Specifically, the moment M_{λ_δ} is the result of the force created from the lateral deformation of the tyre and is given as

$$M_{\lambda_\delta} = (l_g) F_{K_\lambda} \cos(\theta) \cos(\phi), \tag{13}$$

where l_g is the distance between the point of attachment of the gear to the fuselage and the ground.

2.3 Tyre kinematics

Equation (4) describes the motion of the tyre under the influence of the strut's torsional and lateral bending. Here, the effect of the deformation resulting from the lateral bending mode is incorporated into the conventional kinematic equation representing the stretched string theory of a tyre [17]. This is important because the natural frequencies of the lateral and torsional modes are typically different and the resultant lateral deformation is an algebraic sum of the deformation caused by both the modes.

From [17], the nonlinear form of the equation describing the kinematics is given as

$$\dot{\lambda} + \frac{V}{L}\lambda = V\sin(\theta) + (e_{\text{eff}} - h)\cos(\theta)\dot{\theta}. \tag{14}$$

The effect of lateral deformation due to lateral bending on the tyre kinematics can be derived in a similar fashion as in the case of a pure torsional mode. Namely, the relationship between the lateral bending angle δ and the lateral deformation λ of the tyre at the leading edge of the contact patch is given by:

$$\dot{\lambda} + \frac{V}{L}\lambda = (l_g)\dot{\delta}\cos(\delta). \tag{15}$$

To obtain the kinematic equation (4), we superimpose the individual effects of the torsional and lateral motions on the tyre deformation, that is, (14) and (15); this modeling step is justified by derivations that are not presented here.

3 Bifurcation analysis

We now perform a bifurcation analysis of the nose landing gear model, (2)–(4), with the continuation software AUTO [5]. Specifically, we consider the dependence of the dynamics on the forward velocity V and the vertical force F_z, where we fix all other system parameters at the realistic values given in Table 1. Our starting point is the transition to shimmy oscillations with varying V, which can be studied by means of one-parameter bifurcation diagrams. We then consider the bifurcation diagram in the (V, F_z)-plane to provide a more global view of the overall dynamics. Representative time histories are presented to discuss the possible motion of the nose landing gear in terms of the contributions of torsion and lateral bending.

3.1 Dynamics as a function of forward velocity

Equations (2)–(4) always have the equilibrium solution $(\psi, \delta, \lambda) = (0, 0, 0)$, which corresponds to straight-line rolling of the tyre. This equilibrium is stable when the forward velocity V and vertical force F_z are very low, but for higher vertical force as the forward velocity is increased it may lose its stability in a Hopf bifurcation resulting in shimmy oscillations. A continuation in V reveals not only the onset of shimmy, but is also able to follow the ensuing steady-state shimmy oscillations to study their stability.

Figure 2 shows two continuations in V for different values of the vertical force F_z; all other parameters are as in Table 1. For $F_z = 150.0$ kN the zero equilibrium (that is, straight-line rolling) is stable for low velocity V, and it becomes unstable in a Hopf bifurcation H_t at $V \approx 4.6\ \mathrm{m\,s^{-1}}$. This Hopf bifurcation is supercritical and, hence, gives birth to a stable periodic orbit corresponding to shimmy oscillations whose amplitude grows quickly with V. It is represented in panel (a1) in terms of the maximum of the torsion angle ψ, and in panel (a2) in terms of the maximum of the lateral bending stroke $\delta^* = l_g \sin(\delta)$ (at ground level). As can be observed from the difference

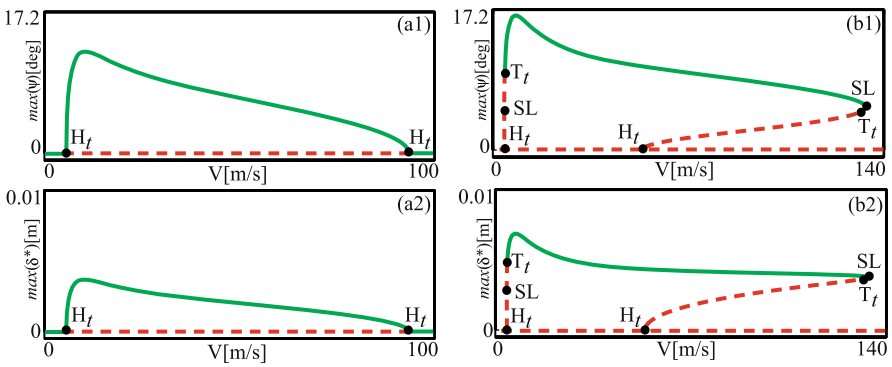

Fig. 2 (Color online) One-parameter continuation in V for $F_z = 150.0$ kN (**a**) and $F_z = 500.0$ kN (**b**); the *top panels* show the maximum of the torsion angle ψ and the *bottom panels* the maximum of the lateral bending stroke δ^*. Stable parts of branches are *solid and green* and unstable parts in *dashed and red*; along the branches one finds Hopf bifurcations H_t (of the torsional mode), saddle-node of limit cycle bifurcations SL, and torus bifurcations T_t (of the torsional mode)

in scale (tens of degrees versus millimeters) of the two panels, the Hopf bifurcation curve H_t corresponds to the undamping of the torsional mode (hence the subscript). The branch of torsional shimmy oscillations is stable throughout and disappears in a second supercritical Hopf bifurcation H_t at $V \approx 93.3\ \mathrm{m\,s^{-1}}$, after which the zero equilibrium of straight-line rolling is stable again. This scenario of onset and disappearance of shimmy oscillations for $F_z = 150.0$ kN is what one also finds for models that only feature a torsional mode and no lateral bending [19].

Figure 2(b) shows the one-parameter bifurcation diagram for $F_z = 500.0$ kN. There are several important differences relative to the case $F_z = 150.0$ kN. The zero equilibrium is now unstable before the Hopf bifurcation H_t. Furthermore, the onset of shimmy oscillations is now due to a subcritical Hopf bifurcation H_t at $V \approx 4.1\ \mathrm{m\,s^{-1}}$, so that the bifurcating shimmy oscillations are initially unstable. On the corresponding branch we find a saddle-node of limit cycle (or fold) bifurcation SL. It is immediately followed by a torus bifurcation T_t at $V \approx 4.3\mathrm{m\,s^{-1}}$ (where a pair of complex conjugate Floquet multipliers of the periodic orbit crosses the unit circle), after which the shimmy oscillations are stable. The branch remains stable over a large range of V, up to a second saddle-node of limit cycle bifurcation SL at $V \approx 133\ \mathrm{m\,s^{-1}}$. Here the branch turns back and, after an immediate torus bifurcation T_t, it connects to the zero-equilibrium at a second subcritical Hopf bifurcation H_t. Since the zero equilibrium does not regain stability, the system jumps from stable shimmy oscillations to some other attractor (not shown) when the velocity V is increased past the rightmost SL point.

Overall, Fig. 2 provides evidence for the interaction between the torsional and lateral bending modes of the landing gear in the form of torus bifurcations for sufficiently high vertical force F_z. More generally, the vertical force F_z has a strong influence on how the behavior of the nose landing gear depends on the forward velocity V. In effect, increasing F_z increases the interaction between the two modes.

3.2 Bifurcation diagram in the (V, F_z)-plane

The bifurcation points that were identified in Fig. 2 can be continued in the (V, F_z)-plane. The result is the two-parameter bifurcation diagram shown in Fig. 3. Its main feature is the interaction between a curve H_t of Hopf bifurcations of the torsional mode and a curve H_l of Hopf bifurcations of the lateral mode.

The torsional Hopf bifurcation curve H_t forms an isola (a closed curve). For lower values of F_z (certainly for $F_z < 450.0$ kN) it is supercritical and leads to stable torsional shimmy oscillations; compare with Fig. 2(a). In fact, this supercritical part of H_t at low vertical force F_z is as presented in Thota et al. [19], where the lateral bending mode was not considered at all. However, the criticality of H_t changes at two degenerate Hopf bifurcation points DH [7, 9], so that the upper part of the isola H_t (in the range $450.0 < F_z < 550.0$ kN) is subcritical. Hence, it gives rise to unstable shimmy oscillations. Two curves SL of saddle-node of limit cycle bifurcations emerge from the codimension-two points DH, and these can be continued towards larger values of F_z until they exit our region of interest. As a consequence, subcritical Hopf bifurcations for small and large velocities V are preceded and followed by saddle-node of limit cycle bifurcations; compare with Fig. 2(b).

The lateral Hopf bifurcation curve H_l in Fig. 3 crosses the bifurcation diagram from left to right. It intersects the torsional Hopf bifurcation curve H_t in two Hopf–Hopf bifurcation points HH at $(V, F_z) \approx (3.8\ \mathrm{m\,s^{-1}},\ 300.0\ \mathrm{kN})$ and $(V, F_z) \approx (154.9\ \mathrm{m\,s^{-1}},\ 274.9\ \mathrm{kN})$. We find that two torus bifurcation curves emerge locally from each of these codimension-two points, which is in agreement with what may be expected from bifurcation theory [7, 9]. More specifically, we find a lower torus bifurcation curve T_l of lateral shimmy oscillations, and a higher torus bifurcation curve T_t of torsional shimmy oscillations, both connecting the two HH points.

The bifurcation diagram in Fig. 3 provides a global picture of the interaction between the torsional and lateral modes. The different bifurcation curves divide the (V, F_z)-plane into regions where different types of solutions are stable. In the white region for low values of F_z there are no shimmy oscillations, that is, the straight-rolling motion is stable. Shimmy oscillations bifurcate when a Hopf bifurcation curve is crossed. As is discussed in Sect. 3.3, the ensuing shimmy oscillation may be of torsional or lateral nature; their respective stability regions are shown in Fig. 3 by right- and left-slanted shading, respectively. It is worth mentioning that size and position of the isola H_t, the points DH and emanating curves SL are almost unaffected by changes of the damping in the lateral mode. Similarly, changes in the torsional damping have very little

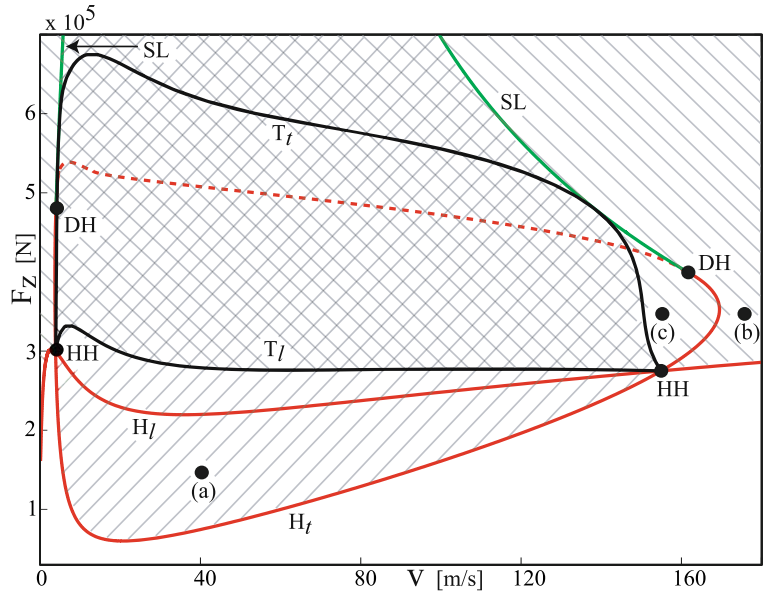

Fig. 3 (Color online) Two-parameter bifurcation diagram of (2)–(4) in the (V, F_z)-plane, consisting of curves of Hopf bifurcations (*red*), saddle-node of limit cycle bifurcations (*green*) and torus bifurcations (*black*). The Hopf bifurcation curve H_t of the torsional mode forms an isola and changes criticality at two degenerate Hopf points DH (the dashed part is subcritical); it interacts with the Hopf bifurcation curve H_l of the lateral mode in two double-Hopf points HH. Time series of shimmy oscillations for the *points* labeled (*a*) to (*c*) are shown in Fig. 5. In the *unshaded* region the zero equilibrium solution (straight-line rolling) is stable, in the region with *right-slanted shading* torsional shimmy oscillations are stable, and in the region with *left-slanted shading* lateral shimmy oscillations are stable; in the checkered region one finds bistability between the two types of shimmy oscillations

effect on the Hopf bifurcation curve H_l. The bifurcation structure in Fig. 3 is in fact typical for the case that damping and stiffnesses of the torsional and lateral modes are more or less of the same order, in which case the curves H_t and H_l cross in two double-Hopf points HH. These codimension-two points act as organizing centers of the dynamics in the sense that they give rise to torus bifurcations that are associated with quasiperiodic shimmy oscillations.

An example of the emergence of shimmy oscillations for large vertical force is provided by the one-parameter continuation in Fig. 4 for $F_z = 650.0$ kN. When the leftmost curve SL in Fig. 3 is crossed in the direction of increasing V, a pair of shimmy oscillations is born, of which the one with the larger amplitude of ψ is stable. The difference in scale of panels (a1) and (a2) of Fig. 4 again shows that the torsional mode dominates. The stable and the unstable shimmy oscillations come together and disappear when the rightmost curve SL in Fig. 3 is crossed. Note also the two torus bifurcations points labeled T_t on the unstable part of the branch. The shimmy oscillations shown in Fig. 4 are no longer connected to the zero equilibrium of straight-rolling motion, because the vertical force of $F_z = 650.0$ kN is above the maximum of the curve H_t. Hence, stable shimmy oscil-

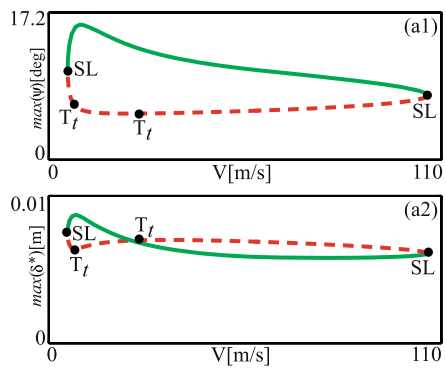

Fig. 4 (Color online) One-parameter continuation in V for $F_z = 650.0$ kN; the *top panel* shows the maximum of the torsion angle ψ and the *bottom panel* the maximum of the lateral bending stroke δ^*. Stable parts of branches are *solid and green* and unstable parts *dashed and red*, with torus bifurcation labeled T_t

lations for $F_z = 650.0$ kN appear and disappear suddenly when the velocity V is changed.

3.3 Different types of shimmy oscillations

We now present different types of shimmy oscillations, which we distinguish in terms of the relative contributions of the torsion angle ψ, the lateral bending stroke δ^* and the lateral deformation of the tyre λ. Figure 5 shows time series of these quantities for the values of the parameters (V, F_z) corresponding to the points labeled (a)–(c) in Fig. 3.

Figure 5(a) shows an example of torsional shimmy oscillations, specifically for $(V, F_z) = (40.0\ \mathrm{m\,s^{-1}}, 150.0\ \mathrm{kN})$, which corresponds to the labeled point (a) in Fig. 3. This point is reached from the stable region by crossing the Hopf bifurcation curve H_t, where the torsional mode undamps. Consequently, we find oscillations of the torsion angle ψ at the frequency (of about 10.6 Hz) of the torsional mode; see Fig. 5(a1). These oscillations induce an oscillation of the lateral tyre deformation λ. Due to the coupling via the tyre, the lateral stroke follows these oscillations with very small amplitude, but there are no oscillations at the frequency of the lateral mode; see Fig. 5(a2). Because of these properties this type of dynamics can indeed be characterized as torsional shimmy oscillations.

Figure 5(b) shows lateral shimmy oscillations for $(V, F_z) = (175.0\ \mathrm{m\,s^{-1}}, 350.0\ \mathrm{kN})$, corresponds to the labeled point (b) in Fig. 3. This type of dynamics can be reached from the stable region by crossing the Hopf bifurcation curve H_l. It is characterized by large amplitude oscillations of the lateral stroke δ^* at its characteristic frequency (of about 16.1 Hz); see Fig. 5(b2). These oscillations again induce an oscillation of the lateral tyre deformation λ, which is now followed by the torsional angle ψ; see Fig. 5(b1). Notice that, compared to the case of torsional shimmy oscillations, the amplitude of ψ is now considerably smaller. Furthermore, ψ simply follows the lateral tyre deformation λ, meaning that the torsional mode frequency is not present in the dynamics. This is why we refer to this dynamics as lateral shimmy oscillations.

Torsional and lateral shimmy oscillations are stable in large regions of the (V, F_z)-plane, which are indicated in Fig. 3 by right-slanted and left-slanted shading, respectively. The region of torsional shimmy oscillations is bounded below by the curve H_t between the two double-Hopf points HH. To the left and the right it is bounded by the first parts of the curve T_t from the points HH up to tangency points of T_t with the saddle-node of limit cycle bifurcation curves SL. The latter curve forms the boundary of the region of stable torsional shimmy oscillations for larger values

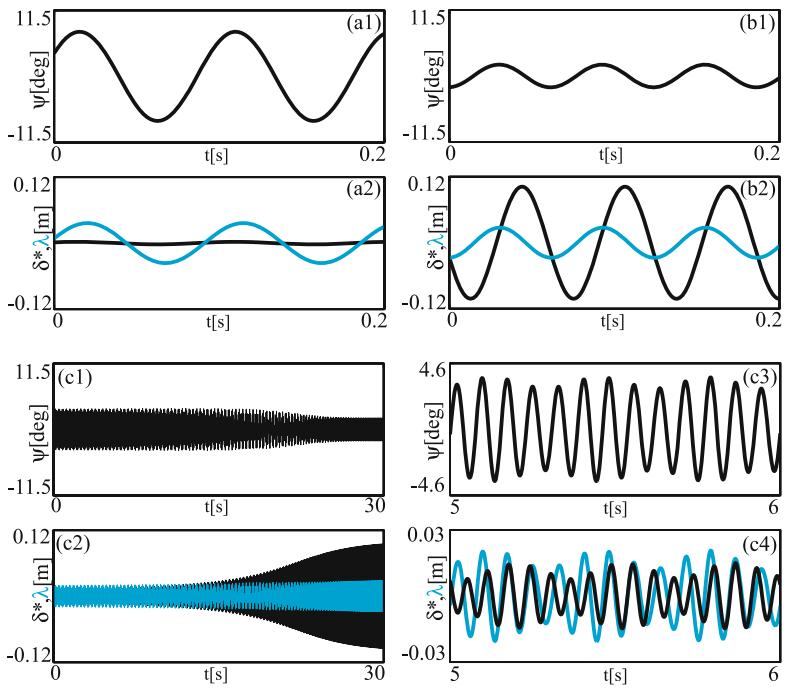

Fig. 5 (Color online) Time series of the torsion angle ψ, and of lateral bending stroke δ^* (*black*) and lateral tyre deformation λ (*blue*) for the values of (V, F_z) that are labelled (a)–(c) in Fig. 3. Specifically, panels (**a**) for $(V, F_z) = (40.0\ \mathrm{m\,s^{-1}}, 150.0\ \mathrm{kN})$ show torsional shimmy oscillations, panels (**b**) for $(V, F_z) = (175.0\ \mathrm{m\,s^{-1}}, 350.0\ \mathrm{kN})$ show lateral shimmy oscillations, and panels (**c**) for $(V, F_z) = (155.0\ \mathrm{m\,s^{-1}}, 350.0\ \mathrm{kN})$ show quasiperiodic shimmy oscillations (on two different time scales) in the transition from torsional to lateral shimmy

of F_z (above about $F_z = 500$ kN). Lateral shimmy oscillations are stable in the region above the union of the torus bifurcation curve T_l and the two parts of the lateral Hopf bifurcation curve H_t to the left of the leftmost point HH and to the right of the rightmost point HH. As a result, there is a large region above the curve T_l where the torsional mode and the lateral mode are both stable. In this bistability region (checkered shading in Fig. 3) the initial condition determines onto which of the two periodic solutions the system settles down. From a practical point of view, there is a clear split of the (V, F_z)-plane. For a light aircraft below a vertical force F_z of about 300 kN, torsional shimmy oscillations are encountered as the only type of dynamical instability. For a heavy aircraft above a vertical force F_z of about 300 kN the situation is quite different: there is a large region of relevant intermediate velocities V between about 5 and 140 m s^{-1} where both types of shimmy oscillations may occur, depending on the initial condition or the path taken into this region. Furthermore, in the bistability region there is the possibility of sudden jumps between stable torsional and stable lateral shimmy oscillations as the result of sufficiently large external perturbations.

Figure 5(c) shows that one may also find shimmy oscillations with components of the frequencies of both the torsional and lateral modes. For the parameter values as specified in Table 1, we find this type of shimmy as a prominent transient phenomenon when the system switches from stable torsional to stable lateral shimmy oscillation as the boundary of bistable regions formed by the torus bifurcation curve T_t is crossed. As Fig. 5(c1)/(c2) shows, in this transition the lateral stroke δ^* increases while that of the torsional mode ψ decreases. At the same time the system switches from the frequency of the torsional mode to the frequency of the lateral mode. The process is quite slow, and one observes both frequency components over several tens of seconds. Due to the notable absence of an observable low rational frequency ratio, we refer to this type of dynamics as quasiperiodic shimmy oscillations. The shorter time series in Fig. 5(c3)/(c4) highlight their quasiperiodic character. We find that quasiperiodic shimmy oscillations can be found transiently whenever the system is moved out of the bistability region by crossing a torus bifurcation curve, which is either T_t to the left or right or T_l when crossing the lower boundary. In the latter case, transient quasiperiodic shimmy is associated with a switch from lateral to torsional shimmy oscillations.

Our numerical investigations indicate that for the parameter values shown in Table 1 we find quasiperiodic shimmy oscillations only as long and physically relevant transients, but not as stable dynamics on an attracting torus. Specifically, the torus bifurcations are subcritical along the curves T_l and T_t, and there do not appear to be other bifurcation curves along which the bifurcating unstable tori stabilize. However, it is to be expected that for different sets of parameter values, corresponding to different aircraft nose landing gears, one may indeed find stable quasiperiodic shimmy oscillations. In particular, it would be an interesting challenge to identify when the torus curves change their criticality; this would require a study of higher-order terms of a suitable Poincaré return map.

3.4 Dependence on the rake angle

The two-parameter bifurcation diagram in the (V, F_z)-plane in Fig. 3 was obtained for the parameter values in Table 1, which were chosen as representative for a midsize passenger aircraft. The question arises how this bifurcation diagram and, in particular, the regions of different types of shimmy oscillations, change when one or several of these parameters are changed. As a parameter of specific interest we consider here the rake angle ϕ for the following reasons. First of all, ϕ may differ quite substantially between aircraft types, in the range between zero to 10 degrees; by contrast, the relative ranges of most other parameters in Table 1 are much smaller. Secondly, the geometric effects of a nonzero rake angle have been incorporated fully into (2)–(4), so that such a study becomes feasible.

Figure 6(a) shows the bifurcation diagram of (2)–(4) in the (V, F_z)-plane for a rake angle of $\phi = 0$. Bifurcation curves and regions of stable straight-rolling, torsional and lateral shimmy oscillations are shown and labeled as in Fig. 3, which is for $\phi = 9$ degrees. The two bifurcation diagrams are qualitatively the same, by which we mean that we find the same bifurcations and regions for both values of ϕ. However, there are clearly differences of a quantitative nature. Most importantly, Fig. 6(a) is shown on a much larger scale, where V now ranges from 0 to 300 m s^{-1} and F_z from 0 to 1000 kN. If viewed in the same range of the (V, F_z)-plane as that shown in Fig. 3, the main difference is that the two torus bifurcation curves T_l and T_t have moved towards larger values of F_z in Fig. 6(a).

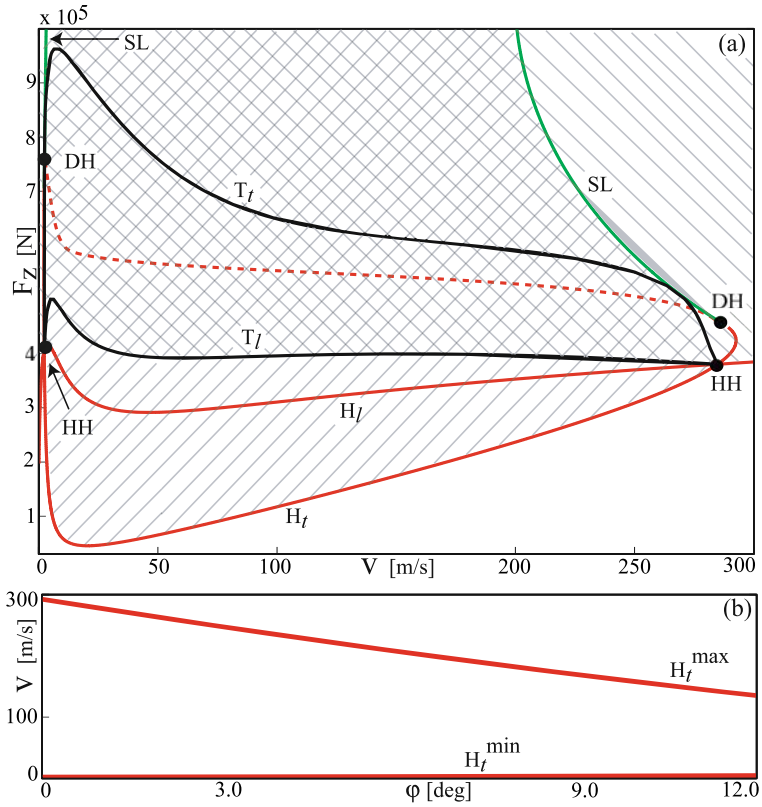

Fig. 6 Panel (**a**) shows the two-parameter bifurcation diagram of (2)–(4) in the (V, F_z)-plane with parameter values as in Fig. 3, but for a zero rake angle ϕ, that is, for $\phi = 0$. Panel (**b**) gives the dependence on ϕ of the leftmost point $H_t^{\min}$ and the rightmost point $H_t^{\max}$ of the Hopf bifurcation curve H_t

The main overall effect of reducing the rake angle appears to be a scaling of the closed Hopf bifurcation curve H_t. This scaling can be quantified on the V-scale by plotting the left- and rightmost points $H_t^{\min}$ and $H_t^{\max}$ of H_t as a function of the rake angle ϕ. As is shown in Fig. 6(b), the points $H_t^{\min}$ and $H_t^{\max}$ scale linearly with ϕ in very good approximation. In particular, $H_t^{\min}$ does not change much at all, while $H_t^{\max}$ moves to lower values of V with increasing rake angle ϕ. This corresponds to a reduced region of bistability between torsional and lateral shimmy oscillations for larger values of ϕ.

4 Discussion and future work

We introduced a mathematical model of an aircraft nose landing gear that takes into account the torsional and the lateral bending modes of the gear. Both are coupled via the interaction through the tyre, which is modeled by incorporating lateral deformation into the classic stretched string model of von Schlippe. In our model we fully incorporate for the first time the geometric effects of a nonzero rake angle of the landing gear. It manifests itself via several nonlinear coupling effects, which include tilting of the tyre during steering and the generation of an effective caster length. While our model is quite general, we considered here the case of an aircraft landing gear, which is characterized by strong damping of torsional and lateral modes and a moderate rake angle.

The main focus of our study was the interaction of torsional and lateral modes of an aircraft landing gear for realistic values of the different model parameters. In particular, the lateral damping was roughly of the same order as that of the torsional mode. We presented a bifurcation diagram in the plane of forward velocity V and vertical force F_z as the two main operational parameters. The bifurcation diagram is organized by Hopf bifurcation curves of the torsional and lateral modes, which cross at two double-Hopf points. These codimension-two bifurcation points effectively organize the interaction of the two modes by giving rise to torus bifurcation curves.

Apart from the well-known torsional shimmy oscillations, we also found stable lateral shimmy oscillations. Both types of shimmy oscillations are stable

in large regions of the (V, F_z)-plane, and there is a large region of bistability between torsional and lateral shimmy oscillations. Furthermore, we found quasiperiodic shimmy oscillations as long transients near curves of torus bifurcations that bound the bistability region. This type of shimmy is characterized by strong frequency components of both the torsional and lateral mode. Shimmy with two frequency components was found in experiments and a 13th-order model of a pulled trailer by Pacejka [11]. More recently, quasiperiodic shimmy has been found by Takács and Stépán [18] in a similar experimental setup of a pulled trailer and in a different mathematical model. Importantly, Stépán shows that in the pulled trailer setup the second frequency is due to a delay effect associated with the rolling tyre, which requires a mathematical model in the form of delay differential equations. By contrast, we found that in an aircraft nose landing gear quasiperiodic shimmy may occur in an ordinary differential equation model due to the interaction of two different modes of the gear itself. We remark that, because of hysteretic damping in the viscoelastic von Schlippe tyre model used here, the tyre response lags behind the strut response by the tyre relaxation time.

The study performed here shows that the different types of shimmy oscillations can be found in a realistic range of forward velocities, that is, below landing and take-off velocities of between 70 and 100 $\mathrm{m\,s^{-1}}$ that are typical for passenger aircraft. From the practical point of view, the influence of the lateral bending mode on the dynamics increases with increasing vertical force on the gear, that is, with loading or braking of the aircraft. For heavy aircraft one may find lateral shimmy as well as quasiperiodic shimmy oscillations as long transients when torsional shimmy oscillations lose their stability. This type of information may have implications for the design of shimmy dampers for aircraft, which are presently designed to dampen only torsional motion.

There are several directions for future research. The landing gear parameters as used in our study are representative of a midsize passenger aircraft. We considered here the influence of the rake angle and showed how the overall scale of the bifurcation diagram changes with the rake angle, while its qualitative features are preserved. A detailed study of the dependence of the bifurcation structure on other parameters, for example, those specifying tyre properties, is the subject of our ongoing research. Secondly, we mention the evaluation of aircraft taxi, take-off and landing scenarios, which involve specific changes of the vertical force as a function of the forward velocity. The relationship between operational parameters can be determined/calibrated from experimental measurements with the goal of investigating more realistic aircraft operation scenarios. Finally, our landing gear model can be expanded to take into account additional oscillatory modes. In the first instance, this would involve modeling oscillations along the strut axis due to oleo (vertical shock absorber) compression. In the longer term, one may also wish to incorporate dynamical modes that are transmitted by the fuselage. The final goal would be the formulation of an integrated mathematical model of a generic aircraft with all landing gear units, but in such a way that a balance is struck between incorporating the relevant effects while keeping the model amenable to bifurcation analysis.

Acknowledgements We thank Hans Pacejka for helpful comments on how to introduce the lateral deformation into the tyre model, and Robert Szalai for his help with the two-parameter continuation of torus bifurcations. This research has been supported by Airbus.

References

1. Baumann, J.: A nonlinear model for landing gear shimmy with applications to the McDonnell Douglas G/A-18A. In: 81st Meeting of the AGARD Structures and Materials Panel (1995)
2. Besselink, I.J.M.: Shimmy of aircraft main landing gears. Dissertation, University of Delft, The Netherlands (2000)
3. Broulhiet, M.G.: La suspension de la direction de la voiture automobile—shimmy et dandinement. Bull. Soc. Ing. Civ. (France) 78 (1925)
4. Dengler, M., Goland, M., Herrman, G.: A bibliographic survey of automobile and aircraft wheel shimmy. Technical report, Midwest Research Institute, Kansas City, MO, USA (1951)
5. Doedel, E.J., Keller, H.B., Kernevez, J.P.: Numerical analysis and control of bifurcation problems, part II: bifurcation in infinite dimensions. J. Bifurc. Chaos Appl. Sci. Eng. **1**(4), 745–772 (1991)
6. Glaser, J., Hrycko, G.: Landing gear shimmy—De Havilland's experience. In: 81st Meeting of the AGARD Structures and Materials Panel (1995)
7. Guckenheimer, J., Holmes, P.: Nonlinear Oscillations, Dynamical Systems and Bifurcations of Vector Fields. Springer, New York (1983)
8. Krabacher, W.E.: A review of aircraft landing gear dynamics. In: 81st Meeting of the AGARD Structures and Materials Panel (1995)
9. Kuznetsov, Y.A.: Elements of Applied Bifurcation Theory. Springer, New York (1995)

10. Pacejka, H.B.: Analysis of the shimmy phenomenon. Proc. Inst. Mech. Eng. 2A **180**(10) (1965–1966)
11. Pacejka, H.B.: The wheel shimmy phenomenon: a theoretical and experimental investigation with particular reference to the nonlinear problem. Dissertation, Delft University of Technology (1966)
12. Pritchard, I.J.: An overview of landing gear dynamics. NASA Technical Reports, NASA/TM-1999-209143 (1999)
13. Smiley, R.F.: Correlation, evaluation, and extension of linearized theories for tyre motion and wheel shimmy. Report submitted to the National Advisory Committee for Aeronautics, Report 1299 (1957)
14. Somieski, G.: Shimmy analysis of a simple aircraft nose landing gear model using different mathematical methods. Aerosp. Sci. Technol. **8**, 1270–9638 (1997)
15. Stépán, G.: Delay, Nonlinear Oscillations and Shimmying Wheels, Kluwer, Dordrecht (1998)
16. Stépán, G.: Chaotic motion of wheels. Veh. Syst. Dyn. **20**(6), 341–351 (1991)
17. von Schlippe, B., Dietrich, R.: Shimmying of a pneumatic wheel. Report submitted to the National Advisory Committee for Aeronautics, NACA TM 1365 (1947)
18. Takács, D., Stépán, G.: Experiments on quasi-periodic wheel shimmy. In: Proc. IDETC/CIE. DETC2007-35336 (2007)
19. Thota, P., Krauskopf, B., Lowenberg, M.: Shimmy in a nonlinear model of an aircraft nose landing gear with nonzero rake angle. In: Proceedings of ENOC (2008)
20. Woerner, P., Noel, O.: Influence of nonlinearity on the shimmy behaviour of landing gear. In: 81st Meeting of the AGARD Structures and Materials Panel (1995)